Kinetics of Sulfur Oxide, Sulfur Fluoride, and Sulfur Oxyfluoride Anions with Atomic Species at 298 and 500 K

Anthony J. Midey*,† and A. A. Viggiano

Air Force Research Laboratory, Space Vehicles Directorate, 29 Randolph Road, Hanscom Air Force Base, Massachusetts 01731-3010

Received: September 21, 2006; In Final Form: January 4, 2007

The rate constants and product-ion branching ratios for the reactions of sulfur dioxide (SO_2^-), sulfur fluoride (SF_n^-), and sulfur oxyfluoride anions ($SO_xF_y^-$) with H, H_2, N, N_2, NO, and O have been measured in a selected-ion flow tube (SIFT). H atoms were generated through a microwave discharge on a H_2/He mixture, whereas O atoms were created via N atoms titrated with NO, where the N had been created by a microwave discharge on N_2. None of the ions reacted with H_2, N_2 or NO; thus, the rate constants are $<1 \times 10^{-12}$ cm^3 s^{-1}. $SO_xF_y^-$ ions react with H by only fluorine-atom abstraction to form HF at 298 and 500 K. Successive F-atom removal does not occur at either temperature, and the rate constants show no temperature dependence over this limited range. SO_2^- and F^- undergo associative detachment with H to form a neutral molecule and an electron. Theoretical calculations of the structures and energetics of HSO_2^- isomers were performed and showed that structural differences between the ionic and neutral HSO_2 species can account for at least part of the reactivity limitations in the $SO_2^- + H$ reaction. All of the $SO_xF_y^-$ ions react with O; however, only SO_2^- reacts with both N and O. $SO_xF_y^-$ reactions with N (SO_2^- excluded) have a rate constant limit of $<1 \times 10^{-11}$ cm^3 s^{-1}. The rate constants for the $SO_xF_y^-$ reactions with H and O are ≤25% of the collision rate constant, as seen previously in the reactions of these ions with O_3, consistent with a kinetic bottleneck limiting the reactivity. The only exceptions are the reactions of SO_2^- with N and O, which are much more efficient. Three pathways were observed with O atoms: F-atom exchange in the reactant ion, F^- exchange in the reactant ion, and charge transfer to the O atom. No associative detachment was observed in the N- and O-atom reactions.

Introduction

Sulfur dioxide (SO_2^-), sulfur fluoride (SF_n^-), and sulfur oxyfluoride anions ($SO_xF_y^-$) have been observed in plasma environments where SF_6, O_2, and H_2O are present in the discharge.[1−5] These ions have also been seen in atmospheric-pressure methane−oxygen flames doped with SF_6 and SO_2.[6,7] Thus, the ion chemistry of these species has been studied to examine their reactivities.[5,8−13] Recently, kinetics experiments have been conducted to determine the formation pathways for these ions, particularly through oxidation by O_3 and O_2.[14,15] Extensive theoretical calculations of the structures and energetics of these ions have augmented these measurements and have helped to explain the observed chemistry.[14,16−21]

Atomic species can also be present in discharge environments, including hydrogen, nitrogen, and oxygen atoms. The kinetics of the reactions of H and H_2 with a variety of cations and anions have been previously studied,[22−27] including a recent study from our laboratory of the reactions of $PO_xCl_y^-$ ions with H and H_2.[28] Analogous surveys of N- and O-atom ion−molecule chemistry have also been done.[8,26,27,29−36] However, the only previous studies of $SO_xF_y^-$ reactions with atoms are for SF_6^- and SF_5^- reacting with H and O,[8,9,13] and only one qualitative measurement of the reaction of SO_2^- with N and O atoms has been made.[10]

To both further the previous flow-tube studies of the oxidation chemistry of $SO_xF_y^-$ [14,15] and better understand the reactivity of these anions, the rate constants and product-ion branching ratios for the reactions of $SO_xF_y^-$ ions with H, H_2, N, N_2, NO, and O have been studied in a selected-ion flow tube (SIFT) at 298 K. The H-atom reactions were also studied at temperatures up to 500 K. In addition, a series of theoretical calculations of the structures and energetics of the possible HSO_2^- isomeric species involved in the associative detachment reaction of SO_2^- with H were performed to better understand the observed chemistry. These results can be compared with the extensive previous calculations of the neutral HSO_2 isomers created through the $H + SO_2$ neutral reaction.[37−49]

Experimental Section

The SIFT has been described in detail elsewhere;[50] however, a brief description follows for the current experiments. $SO_xF_y^-$ ions were generated by electron impact on appropriate reagent gases in a remote source chamber. The desired reactant ion was selected with a quadrupole mass filter and then injected into a fast flow of helium buffer gas (AGA, 99.995%) in the temperature-controlled flow tube. After thermal equilibration, the neutral reactant was introduced into the reaction region. After reaction over a known distance for a previously measured reaction time, the remaining reactant ions and all of the product ions were sampled through a blunt-nose cone containing a small aperture, then analyzed with a second quadrupole mass filter, and detected with a conversion dynode electron multiplier.

* To whom correspondence should be addressed. E-mail: Anthony.Midey@hanscom.af.mil.

† Under contract to the Institute for Scientific Research, Boston College, Chestnut Hill, MA 02467.

10.1021/jp066198c CCC: $37.00
Published on Web 02/17/2007

The H-atom reactions were also studied at 500 K in a previous flow tube with decades of use. However, the O-atom reactions required very clean surfaces to minimize charging effects. Measuring the O-atom reactions in the old flow tube was problematic in that ion signals slowly disappeared, presumably because of surface oxidation creating insulating surfaces. Therefore, the measurements were conducted in a newly constructed stainless steel flow tube that used improved vacuum seals to allow future temperature-dependent studies to be made up to 900 K when heating upgrades are completed. Also, a solid-graphite nose cone was used for the N- and O-atom experiments to further decrease charging effects caused by O-atom reactions on the sampling surface. This nose cone replaced the graphite-coated stainless steel version used in previous experiments.

Various combinations of source gases were required to generate the different sulfur oxide, sulfur fluoride, and sulfur oxyfluoride anions,[14] and they are briefly described as follows: SF_6 (Matheson, 99.99%) was used to generate F^-, SF_5^-, and SF_6^-, whereas neat SO_2 (Matheson, 99.98%) was used to generate SO_2^-. Gas mixtures of 1−5% SF_6 in He were used whenever possible to prolong the lifetime of the rhenium and filaments used in the electron-impact ion source with this gas. Thoriated iridium filaments were alternatively used when oxygen-containing reagents were present. However, pure SF_6 was also used to increase the ion production as needed. SO_2F^- and $SO_2F_2^-$ were created using a mixture of 1% SF_6 in He combined with a small amount of SO_2 in the source. SOF_4^- and SOF_3^- were generated through the association reaction of SF_6^- and H_2O. This chemistry required introduction of the room-temperature vapor pressure from a distilled-water sample along with a mixture of 1% SF_6 in He into a source block cooled to 262 K. Dissolved gases were removed from the water through several freeze−pump−thaw cycles.

Hydrogen atoms were generated via microwave discharge on a mixture of H_2 (Liquid Carbonics, 99.999%) and He in a Pyrex tube, giving typical H-atom dissociation fractions of around 5−10%.[28] The H_2 flow was scanned while the helium flow and microwave power were kept fixed in order to vary the H-atom concentration. Given the relatively small amount of dissociation, most of the H_2 remained and was introduced into the flow tube. Consequently, the reactions of $SO_xF_y^-$ with H_2 were measured first. The concentration of H atoms at 298 K was calibrated using the known rate constant for $F^- + H$ at 298 K.[13] This value had not been determined at 500 K. Therefore, a mixture of CF_2Br_2 (Matheson, >99%) and SF_6 was added to the source to simultaneously generate Cl^- and F^- in order to establish a value for the $F^- + H$ rate constant relative to the known $Cl^- +$ H rate constant at 500 K.[51] The F^- rate constant at 500 K could then be used to calibrate the H-atom concentration for determining the other rate constants at this temperature. Rate constants for the H_2 reactions had relative uncertainties of ±15% and absolute uncertainties of ±25%, and the H-atom reactions had relative uncertainties of ±20% and absolute uncertainties of ±30%.[28]

Oxygen atoms were generated by titrating N atoms with NO (Matheson, 99.5%), where the N atoms had been created via microwave discharge on pure N_2 (AGA, 99.999%).[36,52,53] The separate reactions of $SO_xF_y^-$ ions with N_2 and NO were measured first because only about 1% dissociation of N_2 occurred in the discharge. This method also required studying the N-atom reactions first. To minimize secondary-ion chemistry at higher NO concentrations, the titration was performed using a 10% mixture of NO in He passed through a molecular sieve trap that minimized the contribution of trace impurities in the NO to the observed reactivity. Rate constants for the N_2 and NO reactions had relative uncertainties of ±15% and absolute uncertainties of ±25%, whereas the N- and O-atom reactions had relative uncertainties of ±25% and absolute uncertainties of ±40%.[52,53] A larger uncertainty in the rate constant for $SF_5^- + O$ was observed because the value approached the lower limit of measurements possible with O atoms using this technique.

The product-ion distributions were obtained by extrapolating the measured branching ratios to zero atom concentration to minimize the effects of any secondary chemistry. As discussed below, most of the ions did not react with N atoms. Therefore, the O-atom concentration was varied simply by changing the NO concentration over the course of the titration. For the reaction of SO_2^- with N, the N-atom concentration was scanned by varying the microwave discharge power at a fixed N_2 flow and by varying the N_2 flow at a fixed microwave discharge power to obtain the N-atom branching ratios. To help differentiate between the products from the N- and O-atom reactions with SO_2^- where both atoms reacted, O atoms were also generated by a microwave discharge on a mixture of 1% O_2 in He while the flow of the mixture was scanned at fixed microwave power to vary the O-atom concentration. This method was utilized previously in the O_2^- and PO_2Cl^- reactions.[52,53] The branching ratios for the major product ions have uncertainties of ±5%.[54]

TABLE 1: Rate Constants and Products for the Reaction of $SO_xF_y^-$ Ions with H Atoms Measured in a Selected-Ion Flow Tube (SIFT) from 298 to 500 K

reactants	products	ΔH_{rxn}^{298K} (kJ mol^{-1})	rate constant (×10^{-9} cm^3 s^{-1}) [k_{col}] 298 K	500 K
$F^- + H$	$HF + e^-$	−242	1.6[a] [2.0]	1.4 [2.0]
$SF_5^- + H$	no reaction		<0.005 [1.9]	<0.005 [1.9]
$SF_6^- + H$	$SF_5^- + HF$	−431	0.31 [1.9]	0.25 [1.9]
$SOF_3^- + H$	no reaction		<0.005 [1.9]	<0.005 [1.9]
$SOF_4^- + H$	$SOF_3^- + HF$	−470	0.18 [1.9]	0.12 [1.9]
$SO_2^- + H$	$HSO_2 + e^-$	38[b]	0.23 [1.9]	0.26 [1.9]
	cis-$HOSO + e^-$	−62[b]		
$SO_2F^- + H$	no reaction		<0.005 [1.9]	<0.005 [1.9]
$SO_2F_2^- + H$	$SO_2F^- + HF$	−388	0.32 [1.9]	0.26 [1.9]

[a] Fehsenfeld et al.[13] [b] ΔH_f^0 for the neutral product from G2 corrected values of Laakso et al.[42]

Results

(a) $SO_xF_y^- + H$ and H_2. Table 1 summarizes the kinetics results for the reactions of $SO_xF_y^-$ ions with H atoms at 298 and 500 K. The heats of reaction at 298 K given in Table 1 were determined from the experimental[55,56] and G2 corrected theoretical[14,42] standard heats of formation at 298 K for the relevant species. None of the ions listed in Table 1 react with H_2. Consequently, an upper limit for the rate constant of $<1 \times 10^{-12}$ cm^3 s^{-1} can be deduced for the H_2 reactions. SF_5^- does not react with H atoms, as seen in previous flowing afterglow experiments.[8] A rate constant of 3.1×10^{-10} cm^3 s^{-1} for the SF_6^- reaction with H was found in the SIFT, which agrees with the flowing afterglow value of 2.7×10^{-10} cm^3 s^{-1} of Fehsenfeld et al.[13] within the experimental uncertainties. All of the rate constants for the H-atom reactions are ≤25% of the Langevin collision rate constant, k_{col}, similar to the reactions of $SO_xF_y^-$ with O_3.[14,15] No temperature dependence of the rate constants was observed over the limited temperature range from 298 to 500 K, within the uncertainty of the measurements.

TABLE 2: Rate Constants and Product Branching Ratios for the Reactions of $SO_xF_y^-$ Ions with N and O Atoms Measured in a Selected-Ion Flow Tube (SIFT) at 298 K[a]

reactants	products	branching ratio	ΔH_{rxn}^{298K} (kJ mol^{-1})	rate constant ($\times 10^{-10}$ cm^3 s^{-1}) [k_{col}]
$SF_5^- + O$	$F^- + SOF_4$	1.00	−150	0.54 [5.6]
$SF_6^- + O$	$O^- + SF_6$	1.00	−41	1.1 [5.5]
$SO_2F^- + O$	$F^- + SO_3$	0.60	−120	1.5 [5.7]
	$SO_3^- + F$	0.40	−4	
$SO_2F_2^- + O$	$SO_3F^- + F$	1.00	−382	0.91 [5.6]
$SO_2^- + N$	$SO^- + NO$	>0.90	−83	1.8 [7.2]
	$S^- + NO_2$	<0.10	41	
$SO_2^- + O$	$O^- + SO_2$	1.00	−34	4.0 [5.9]
$SOF_3^- + O$	$SO_2F_2^- + F$	1.00	−11	0.77 [5.6]
$SOF_4^- + O$	$F^- + (SO_2F_2 + F)$	1.00	−60	0.79 [5.6]

[a] None of the ions listed above, excluding SO_2^-, react with N atoms; therefore, $k < 1 \times 10^{-11}$ cm^3 s^{-1}.

The major reaction pathway with H atoms is F-atom abstraction to form HF as given by

$$SO_xF_y^- + H \rightarrow SO_xF_{y-1}^- + HF \quad (1)$$

However, successive halogen-atom abstraction from the product ions was not observed as previously seen in the reactions of $PO_xCl_y^-$ with H to form HCl,[28] despite the fact that the primary $SO_xF_y^-$ product ions in Table 1 have spin-allowed exothermic channels to form HF.

Associative detachment of H to the reactant ion to form a neutral product and an electron is the other reaction pathway seen. This channel can be monitored by measuring the total ion current at the nose-cone aperture and the total reactant and product-ion counts at the detector as a function of H-atom concentration. If electrons and neutral molecules are produced rather than ions, both the total ion counts detected and the nose-cone current observed will decrease as the H-atom concentration increases because electrons rapidly diffuse to the flow-tube walls and are not be collected at the nose cone. Only F^- and SO_2^- react with H atoms in this manner. The details of the SO_2^- reaction to form HSO_2 products will be addressed in detail later.

(b) $SO_xF_y^-$ + N, N_2, NO, and O. Table 2 summarizes the kinetics results for the reactions of $SO_xF_y^-$ ions with N and O atoms at 298 K. The heats of reaction at 298 K given in Table 2 were similarly determined from the experimental[55,56] and corrected G2 method theoretical[14,42] standard heats of formation at 298 K for the relevant species. None of the ions react with N_2 and NO. Thus, the upper limit for both the N_2 and NO rate constants could be given as $<1 \times 10^{-12}$ cm^3 s^{-1}. Only SO_2^- reacts with both N and O. The remaining $SO_xF_y^-$ ions do not react with N atoms, the rate constant being $<1 \times 10^{-11}$ cm^3 s^{-1}. This limiting value is higher than that for H atoms because only ca. 1% dissociation of N_2 occurs, leading to lower absolute total N- and O-atom concentrations,[52,53] which are 5−10 times lower than those achievable with H atoms.

Neither SF_6^- nor SF_5^- reacts with N atoms. SF_6^- is found to charge transfer to O atoms with a rate constant of 1.1×10^{-10} cm^3 s^{-1}. This value is about a factor of 2 higher than that for the SF_5^- reaction of 5.4×10^{-11} cm^3 s^{-1}, which produces F^- and SF_4O. A previous measurement of the SF_6^- rate constant by Fehsenfeld[8] in a flowing afterglow (5×10^{-11} cm^3 s^{-1}) is a factor of 2 lower than the present value. Considering that the previous measurement reported a factor of 2 uncertainty, these values are in agreement. Hunton et al.[9] measured the ratio of the SF_6^- and SF_5^- rate constants to be 5:1. In those experiments, an SF_5^- rate constant was determined to be 1.1×10^{-11} cm^3 s^{-1} based on the Fehsenfeld value for SF_6^-. Using the present value, one finds that the Hunton et al. value for SF_5^- increases to 2.2×10^{-11} cm^3 s^{-1}, reducing the discrepancy to a factor of 2.4. As mentioned previously, this rate constant is approaching the lower limit that can be determined with O atoms, and a factor of 2 difference might be all that is possible.[52,53]

Examining Table 2, three major reaction pathways arise in the reactions of $SO_xF_y^-$ with O atoms. These channels are given by the equations

$$SO_xF_y^- + O \rightarrow SO_{x+1}F_{y-1}^- + F \quad (2a)$$

$$SO_xF_y^- + O \rightarrow F^- + SO_{x+1}F_{y-1} \quad (2b)$$

$$SO_xF_y^- + O \rightarrow O^- + SO_xF_y \quad (2c)$$

Exchange of a F atom for an O atom in the reactant ion as shown in eq 2a is one major pathway and is observed in the SO_2F^-, $SO_2F_2^-$, and SOF_3^- reactions. Another major reaction channel involves loss of F^- from the reactant ion with concomitant incorporation of the O atom into the corresponding neutral fragment as given in eq 2b. This pathway was seen with SF_5^-, SO_2F^-, and SOF_4^-. Reactions 2a and 2b differ only in which fragment has the negative charge. Charge transfer to form O^- is the third reaction pathway, and it is the only product channel seen with SF_6^- and SO_2^-. This observation is consistent with the electron affinities (EAs) of the corresponding neutral SO_xF_y species.[14,16] Only SF_6 and SO_2 have EA values (~1.1 eV) that are below the oxygen atom EA of 1.46 eV.[55] Grabowksi et al. observed only O^- products in analogous experiments on $SO_2^- + O$ in a flowing afterglow, performed using both N-atom titration and O_2/He discharge generation to make O atoms. However, those experiments were performed to bracket the EA of SO_2, and rate constant measurements were not made.[10] In addition, the neutral products for the SOF_4^- reaction are given in parentheses in Table 2 because calculations of the SO_2F_3 structure and energetics showed that it is metastable with respect to dissociation into SO_2F_2 and F as shown.[14,17]

No associative detachment was observed with any of the ions during the titration experiments. Associative detachment with O atoms is >34 kJ mol^{-1} endothermic for all of the ions except SO_2^-, for which the process to generate SO_3 is 241 kJ mol^{-1} exothermic. However, although sampling issues from O-atom interactions with the nose-cone surface were minimized, small effects cannot be completely eliminated. These effects can create difficulties in accurately measuring small changes in the nose-cone current that would indicate the production of rapidly diffusing electrons in the flow tube from associative detachment. Therefore, a minor contribution from associative detachment cannot be ruled out in the SO_2^- and O reaction.

Product identification in the SO_2^- reactions proved difficult. Only O^- was observed as a product when the O_2/He discharge method was used, and this ion was assigned as the only product in the O-atom reaction. In the N_2 discharge, both $m/z = 32$ and 48 ions were observed from N-atom reaction, where the latter product can be assigned to SO^-. The former product is S^-, at least partially generated as a secondary ion from the reaction of SO^- with N, especially given that it increases with increasing N-atom concentrations. Extrapolating to zero N-atom concentration, the 32 amu product ion still appears to account for roughly 10% of the total primary products from SO_2^-. Producing S^- from $SO_2^- + N$ is 41 kJ mol^{-1} endothermic, which is roughly energetically possible given the average thermal kinetic and rovibrational energy[57−59] available in the $SO_2^- + N$ reaction

system at 298 K. The reaction of SO_2^- with N to generate O_2^- and NS is 151 kJ mol^{-1} endothermic, eliminating that possibility. These observations most likely indicate that the secondary reaction of SO^- with N is quite a bit faster than the SO_2^- reaction, but direct production of S^- cannot be ruled out. Therefore, only limits for the branching ratios are given in Table 2.

Discussion

(a) $PO_xCl_y^-$ vs $SO_xF_y^-$ Reactivity with H, N, and O Atoms. No temperature dependence of the rate constants and product branching ratios was observed for the reactions of both $SO_xF_y^-$ and $PO_xCl_y^-$ ions[28] with H atoms from 298 to 500 K. In addition, the rate constants for both the $SO_xF_y^-$ and $PO_xCl_y^-$ reactions with H were all ≤25% of the Langevin collision rate constant from 298 to 500 K. These observations are similar to the reactivity trends observed in the reactions of $SO_xF_y^-$ ions with O_3,[14,15] where a kinetic bottleneck hinders the reactivity, despite the availability of highly exothermic spin-allowed reaction pathways. Although ion−molecule reactions that seem to violate spin conservation have been observed that still have large rate constants,[60] a similar kinetic bottleneck as in the O_3 reactions also appears to limit the rate constants for these systems reacting with H atoms. The current observations might indicate that the intermediate lifetime is short and that the reactants cannot sample the whole reactive surface. The small polarizabilities of these neutrals would be consistent with this possibility.

The primary $SO_xF_{y-1}^-$ product ions shown in Table 1 formed via eq 1 do not undergo an additional removal of F atom, in contrast to the successive Cl atom removal with the $PO_xCl_y^-$ ions.[28] The reactivity pattern observed here follows the bond order of the central S atom in the reactant ion (defined as the sum of twice the number of S−O bonds plus the number of S−F bonds) as also seen in reactions with O_3.[14,15] In that work, the $SO_xF_y^-$ ions with an even number of total bonds react, whereas the ions with an odd number of bonds do not. The secondary reactions of the main product ions to form another HF molecule are both exothermic and spin-allowed. However, the primary product ions with odd numbers of bonds are closed-shell stable species, limiting their reactivity.

In contrast to the H-atom reactions, all of the $SO_xF_y^-$ ions react with O atoms. Interestingly, the rate constants for the O-atom reactions with all of the anions are again ≤25% of the Langevin collision rate constant, the exception being SO_2^- and maybe SO^-. The similar trends in reaction efficiency as seen with H and O_3 indicate that an analogous kinetic bottleneck exists in this system, possibly indicative of common features of the respective potential energy surfaces.

(b) SO_2^- Ion Chemistry. As seen in Table 1, associative detachment of H atoms to SO_2^- produces neutral HSO_2 products. The structures and energetics of the various neutral HSO_2 isomers have been extensively studied both experimentally[37−41] and theoretically.[37−49] However, the anion that could be temporarily created during the associative detachment involving H atoms has not been characterized. Consequently, structure and energetic calculations for the potential isomers of the HSO_2^- ions were performed using Gaussian 03.[61]

Recently, high-level calculations of the H + SO_2 ground-electronic-state potential energy surface were made by Ballester and Varandas using double many-body expansion (DMBE) methods fit to ab initio full-valence complete-active-space calculations at the FVCAS/aug-cc-pVDZ and aug-cc-pVTZ levels.[45] Napolion and Watts also recently performed coupled-cluster calculations of the structures and energetics for the HSO_2 and HOSO isomers at the CCSD(T) level with several basis sets. However, analogous calculations at these levels of theory for the HSO_2^- anion structures are beyond the scope of the current study. Consequently, a series of less computationally expensive calculations were made for the isomers of HSO_2^- ion at the same levels of theory previously utilized for probing the corresponding neutral HSO_2 isomers.[37,43,44,46] Using the same levels of theory affords meaningful comparisons of the results for the anion and neutral species.

The energetics were calculated at the G2 level for direct comparison with the G2 calculations of the neutral structures on the H + SO_2 potential energy surface,[42,43] as well as the thermochemistry of the $SO_xF_y^-$ ions and neutrals calculated using G2 theory.[14,17] Optimized geometries and harmonic vibrational frequencies for the anionic HSO_2^- isomers were calculated at the HF/6-31G(d) level, with further geometry optimization of these structures at the MP2(Full)/6-31G(d) level as part of the G2 calculation. In addition, density functional theory (DFT) computations of the structures and vibrational frequencies were performed at the B3LYP/6-311G(d,p) level, which follows a series of HF and MP2 computations by Qi et al. for the neutral H + SO_2 potential surface using this basis set.[44]

To also examine the effects of electron correlation that have been observed in neutral HSO_2 isomer calculations even at high levels of theory,[42,46,47,49] computationally inexpensive MP2 geometry optimizations and vibrational frequency calculations for the singlet HSO_2^- isomers were also performed at the MP2/6-311++G(2d,2p) level. These results can be directly compared to the corresponding MP2 neutral structure results of Isoniemi et al.[37] that employed this larger basis set. The optimized structural parameters are reported in Table 3 for several different methods as defined by the diagram in Figure 1. The G2 0 K energies and 298 K enthalpies are listed in Table 4, along with the corresponding G2(MP2) values. The G2 energies in Table 4 of the structures given in Table 3 at the MP2(Full)/6-31G(d) level in the G2 method are plotted in Figure 2 relative to the lowest-energy HSO_2^- ion. Wavefunction stability was verified at the HF, B3LYP, and MP2/6-311++G(2d,2p) levels of theory for all of the ions listed in Table 3.

Two stable minimum-energy structures exist for singlet-electronic-state HSO_2^- anions. The global minimum-energy structure has an HSO_2^- form with the H bound to the S atom out of the plane. The other lowest-energy structure has an $HOSO^-$ arrangement with the H atom out of the plane. Both the *cis*- and *trans*-$HOSO^-$ planar structures were found to be transition states. The neutral *trans*-HOSO structure has been shown to be a transition state to rotation of the H atom around the S−O bond.[37,42,44−47,49] Both the cis and trans ionic transition-state structures have an O−H wag as the imaginary frequency, indicating that these structures play similar roles. In addition, all four methods agree that $HOSO^-$ is nonplanar. All of the methods also showed that the neutral HOSO arrangement of atoms is the global minimum for all of the neutral structures. With the neutral HOSO arrangement, whether the actual structure of the global minimum is a nonplanar HOSO or a cis planar HOSO geometry depends on the theoretical method and the basis set used.[37,42,44−47,49] Despite the unresolved issue of whether the neutral HOSO global minimum-energy structure is planar or not, the energy difference between the planar and nonplanar HOSO structures at the CCSD(T) level of theory is <1 kJ mol^{-1}.[49] The $HOSO^-$ ions are 15−47 kJ mol^{-1} higher in energy than the HSO_2^- ions, depending on the level of theory used. A third transition-state structure having a planar C_{2v} HSO_2

TABLE 3: Bond Lengths and Bond Angles Calculated for the HSO_2^- Isomers at Different Levels of Theory Grouped by Method[a]

ion	r(H−S) (Å)	r(H−O) (Å)	r_1(O−S) (Å)	r_2(O−S) (Å)	−HOS (deg)	−OSO (deg)	−HOSO (deg)	method/ref
$^1HOSO^-$		0.949	1.726	1.538	105.3	107.3	64.2	HF/6-31G(d)
$^3HOSO^-$		0.951	2.160	1.537	101.8	146.1	−44.9	
^2HOSO		0.969	1.655	1.468	111.5	108	59.5	Binns and Marshall[b]
$^1HOSO^-$		0.975	1.807	1.563	102.0	110.2	71.0	MP2(Full)/6-31G(d)
$^3HOSO^-$		0.975	2.112	1.580	101.6	169.2	0.0	
^2HOSO		0.983	1.661	1.482	106.9	109.8	0.0	Laakso et al.[c]
$^1HOSO^-$		0.962	1.809	1.556	101.3	108.2	76.1	MP2/6-311++G(2d,2p)
^2HOSO		0.969	1.655	1.475	106.3	109.0	0.1	Isoniemi et al.[d]
$^1HOSO^-$		0.964	1.834	1.567	101.8	109.7	71.2	B3LYP/6-311G(d,p)
$^1HSO_2^-$	1.379		1.492	1.492	101.3	114.8		HF/6-31G(d)
$^2HSO_2$	1.339		1.439	1.439	106.6	123.6		Binns and Marshall[b]
$^1HSO_2^-$	1.432		1.521	1.521	101.1	115.7		MP2(Full)/6-31G(d)
$^1HSO_2^-$	1.401		1.519	1.519	100.1	114.2		MP2/6-311++G(2d,2p)
$^2HSO_2$	1.366		1.461	1.461	106	124.6		Isoniemi et al.[d]
$^1HSO_2^-$	1.469		1.523	1.523	101.0	114.6		B3LYP/6-311G(d,p)
				ion transition states				
cis-$^1HOSO^-$		0.951	1.739	1.549	100.2	102.7	0	HF/6-31G(d)
		0.979	1.821	1.573	95.0	103.5	0	MP2(Full)/6-31G(d)
		0.968	1.821	1.566	95.3	102.2	0	MP2/6-311++G(2d,2p)
		0.968	1.847	1.577	96.3	104.2	0	B3LYP/6-31G(d,p)
trans-$^1HOSO^-$		0.950	1.758	1.532	105.8	104.1	180.0	HF/6-31G(d)
trans-^2HOSO		0.952	1.632	1.456	105.3	110.1	180.0	Binns and Marshall[a]
		0.977	1.852	1.558	99.6	107.4	180.0	MP2(Full)/6-31G(d)
		0.966	1.858	1.547	100.2	104.5	180.0	MP2/6-311++G(2d,2p)
		0.966	1.884	1.561	99.3	107.2	180.0	B3LYP/6-31G(d,p)

[a] Structural parameters from the literature for the corresponding neutral HSO_2 isomer calculated at the same level of theory are shown in italics. [b] Reference 46. [c] Reference 42. [d] Reference 37.

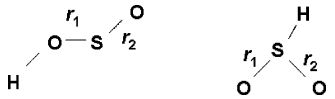

Figure 1. Structural parameters defined for the $HOSO^-$ and HSO_2^- ions as given in Table 3.

arrangement was also found using all of the methods listed in Table 3. However, a wavefunction instability arises with all of the methods; thus, it is not discussed further.

A search for stable triplet-electronic-state HSO_2^- isomers shows that two stable geometries can be found using the HF and MP2 optimizations from the G2 calculations. The lower-energy triplet structure has an $HOSO^-$ arrangement, lying 155 kJ mol^{-1} above the singlet HSO_2^- global minimum and 104.5 kJ mol^{-1} above the singlet $HOSO^-$ isomer. The other geometry found is essentially a very weakly bound planar complex with an HSO_2^--type arrangement having an SO_2^- moiety with a H−S distance of 3.191 Å. This complex is comparable in energy to the reactants, which is consistent with having the H atom positioned at such a great distance. The wavefunctions are stable at the HF/6-31G(d) level for both species.

Examining the structures in Table 3, all of the singlet HSO_2^- bond lengths at the different levels of theory are around 0.04−0.06 Å longer than those in neutral HSO_2. The S−O bonds in both the neutral species and the anion are consistent with S−O double bonds. The SO_2 moiety in HSO_2^- is also structurally similar to neutral SO_2.[57,58] The singlet- and triplet-state $HOSO^-$ ions have a slightly shorter O−H bond than the neutral species. However, the middle S−O single bonds in both the singlet and triplet isomers are substantially longer (>0.07 Å) than those in neutral HOSO. The terminal S−O bond is closer in length to a S−O double bond, but it is also over 0.07 Å longer than in the neutral species. In fact, the central S−O bond in triplet $HOSO^-$ is 2.112 Å, suggesting that this species is more like an [OH−SO]$^-$ complex. The OSO bond angles in singlet $HOSO^-$ and neutral HOSO are within ca. 1° of each other, but the triplet anion has an almost-linear OSO arrangement. In addition, the HOS bond angle is 3−5° lower in both the singlet- and triplet-state ions.

As seen in Table 1, the reaction of SO_2^- with H to from HSO_2 is 38 kJ mol^{-1} endothermic, which is barely energetically accessible at 298 K given the translational and rovibrational energy available to the reactants,[57−59] whereas formation of planar *cis*-HOSO would be 63 kJ mol^{-1} exothermic. These reaction enthalpies were determined using the heats of formation at 298 K of Laakso et al. based on G2 theory for HSO_2 and HOSO with a ±10 kJ mol^{-1} uncertainty as derived from the reaction thermochemistry of several neutral reactions.[42] However, the DFT heat of formation value at 298 K of Denis and Ventura for HSO_2 was evaluated to be 36.8 kJ mol^{-1} lower according to a series of calculations at the B3LYP and B3P91W levels using various-size basis sets for several reaction sequences. This value has an uncertainty of ±8 kJ mol^{-1}.[48] Using the DFT value indicates that H + SO_2^- would be only around 1 kJ mol^{-1} endothermic to form HSO_2, compared to 4 kJ mol^{-1} exothermic for HSO_2 using an experimental estimation of ΔH_f^{298K} gleaned from S−H bond energies measured through chemiluminescence studies of $SO_2/H_2/N_2/O_2$ flames.[62−64] In spite of this range of values, associative detachment to form the neutral HSO_2 isomeric form is energetically feasible at 298 K.

Using the G2 heats of formation for the singlet HSO_2^- and $HOSO^-$ isomers given in Table 4 calculated from the atomization method based on the G2 0 K energies and 298 K enthalpies of Laakso et al.,[42] the reactions of H with SO_2^- to produce HSO_2^- and $HOSO^-$ ions are 219 and 270 kJ mol^{-1}

TABLE 4: Energetics for the HSO_2^- Isomers Calculated Using G2 and G2(MP2) Theory, Including the Vertical Detachment Energy (VDE) of the Anion and the Electron Affinity (EA) for the Adiabatic Neutral Transition

ion	G2 (0 K) energy (hartrees)	G2 (298 K) enthalpy (hartrees)	ΔE (0 K) G2 (kJ mol^{-1})	G2(MP2) (0 K) energy (hartrees)	G2(MP2) (298 K) enthalpy (hartrees)	ΔE (0 K) G2(MP2) (kJ mol^{-1})
$^1HSO_2^-$	−548.639 560	−548.635 400	0	−548.629 573	−548.625 412	0
vertical $^2HSO_2$	−548.531 208[a]			−548.521 787[a]		
$^1HOSO^-$	−548.621 823	−548.617 035	46.6	−548.609 731	−548.604 943	52.1
vertical ^2HOSO	−548.516 703[b]			−548.506 891[b]		
cis-$^1HOSO^-$	−548.618 691	−548.614 278	54.8	−548.606 765	−548.602 352	59.9
trans-$^1HOSO^-$	−548.612 592	−548.608 174	70.8	−548.600 356	−548.595 939	76.7
$^3HOSO^-$	−548.582 037	−548.576 281	151.0	−548.570 411	−548.564 655	155.3

	ΔH_f^{298K} G2 (kJ mol^{-1})	VDE G2 (kJ mol^{-1})	ΔH_f^{298K} G2(MP2) (kJ mol^{-1})	VDE G2(MP2) (kJ mol^{-1})
$^1HSO_2^-$	−389.1	258.5	−413.8	256.9
$^1HOSO^-$	−340.9	284.5	−360.0	283.0

	G2 EA[c] (kJ mol^{-1})	G2(MP2) EA[d] (kJ mol^{-1})
$^2HSO_2$	276.0	270.0
^2HOSO	109.6	103.2

[a] Geometry of the HSO_2^- anion. [b] Geometry of the $HOSO^-$ anion. [c] G2 (0 K) neutral energies from Laakso et al.[42] [d] G2(MP2) (0 K) neutral energies from Frank et al.[40]

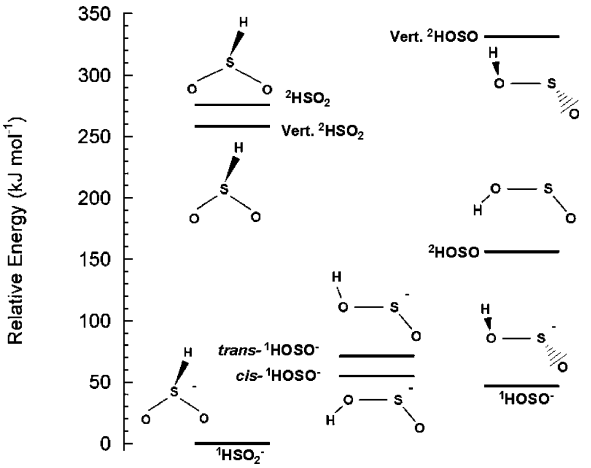

Figure 2. Energies of the isomers of HSO_2 and HSO_2^- species in kJ mol^{-1} plotted relative to the minimum-energy HSO_2^- ion structure. The energies were calculated at the G2 level of theory as shown in Table 4 and the references therein for the structures given in Table 3 optimized at the MP2(Full)/6-31G(d) level in the G2 method.

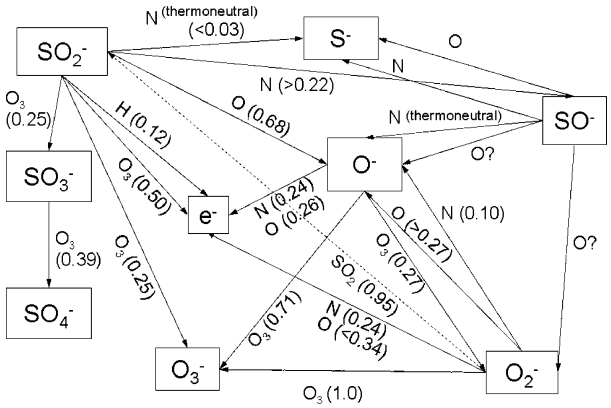

Figure 3. Cycle of SO_2^- ion−molecule chemistry combining the current results with previous measurements from refs 14, 15, 53, and 65−68. The numbers in parentheses are the products of the branching ratio for the product channel with the reaction efficiency, where the efficiency is defined as the ratio of the observed rate constant, k, to the collision rate constant, k_{col}.

exothermic, respectively. However, as seen in Table 4, if neutral HSO_2 is produced via vertical electron detachment from HSO_2^-, the reaction would require 26 kJ mol^{-1} more energy than the adiabatic process. An even greater difference of over 100 kJ mol^{-1} (>1 eV) in energy is found for the vertical vs adiabatic processes with $HOSO^-$. Thus, given the differences in the anionic and neutral structures, the detachment process might access parts of the neutral potential energy surface where the Franck−Condon factors are not favorable under the current reaction conditions. This possibility would be even greater for the triplet $HOSO^-$ isomer that has a substantially different structure than any of the local minima on the HSO_2 surface. These observations are consistent with the observed H-atom rate constant being <25% of the collision rate constant, creating a kinetic bottleneck. Furthermore, large barriers to both formation of HOSO from H + SO_2 and to isomerization from HSO_2 to *cis*-HOSO have been found.[37,40,43−45] Similar barriers might arise on the anionic singlet potential surface that would also hinder the reaction. The G2(MP2) EA and vertical detachment energy (VDE) values given in Table 4 derived from the neutral energies of Frank et al.[40] are <7 kJ mol^{-1} different from the G2 values for both systems, so the qualitative arguments still hold. Detailed scans of the potential energy surface for the anions are beyond the scope of the current work.

Combining the current experimental results with previous ion chemistry measurements at 298 K,[14,15,53,65−68] an overview of the interrelated pathways for the SO_2^- oxidation products can be derived as shown in Figure 3. The numbers in parentheses are reaction efficiencies determined using the equation

$$\text{reaction efficiency} = f\frac{k}{k_{col}} \qquad (3)$$

where f is the branching ratio for a given product channel generated by a reaction with total rate constant k and k_{col} is the Langevin collision rate constant. As seen in Figure 3, a complicated series of reactions generating a wide variety of ionic

products can arise if both SO_2^- ions and atomic species are present. Thus, a complete description of this chemistry would require accounting for the numerous reaction channels shown in Figure 3.

Conclusions

The rate constants and product-ion branching ratios for the reactions of $SO_xF_y^-$ ions with H, H_2, N, N_2, NO, and O have been measured in a SIFT. None of the ions reacts with H_2, N_2, and NO; thus, the rate constants are $<1 \times 10^{-12}$ cm^3 s^{-1}. All of the $SO_xF_y^-$ ions react with O; however, only SO_2^- reacts with both N and O. The rate constants for $SO_xF_y^-$ reactions with H and O at 298 K are $\leq$25% of the collision rate constant as seen previously for O_3 reactions with these ions, consistent with a kinetic bottleneck that has been found to limit the reactivity. The only exceptions are the reactions of SO_2^- with N and O, which are much more efficient.

$SO_xF_y^-$ ions react with H solely via fluorine-atom abstraction to form HF at 298 and 500 K. Successive F-atom removal does not occur at either temperature, and the rate constants show no temperature dependence over this limited range. Three pathways were observed with O atoms: F-atom exchange in the reactant ion, F^- exchange in the reactant ion, and charge transfer to the O atom. Associative detachment was observed only in the reactions of SO_2^- and F^- with H atoms. Theoretical calculations of the HSO_2^- isomeric structures were performed to understand the reaction mechanism for detachment. The calculations show that structural differences between the ionic and neutral HSO_2 species can account for the reactivity limitations observed in the $SO_2^- + H$ reaction through the rate constants.

Acknowledgment. We thank Thomas Miller for helpful discussions and John Williamson and Paul Mundis for technical support. This work was supported by the Air Force Office of Scientific Research under Program EP2303A. A.J.M. was supported through Boston College under Contract FA8718-04-C-0006.

References and Notes

(1) Sauers, I. *Plasma Chem. Plasma Processes* **1988**, *8*, 247.
(2) Sauers, I.; Harman, G. *J. Phys. D: Appl. Phys.* **1992**, *25*, 774−782.
(3) Sauers, I.; Harman, G. *J. Phys. D: Appl. Phys.* **1992**, *25*, 761.
(4) Van Brunt, R. J.; Herron, J. T. *IEEE Trans. Electr. Insul.* **1990**, *25*, 7594.
(5) Van Brunt, R. J.; Sieck, L. W.; Sauers, I.; Siddagangappa, M. C. *Plasma Chem. Plasma Processes* **1988**, *8*, 225.
(6) Goodings, J. M.; Bohme, D. K.; Elguindi, K.; Fox, A. *Can. J. Chem.* **1986**, *64*, 689−694.
(7) Karellas, N. S.; Goodings, J. M. *Int. J. Mass Spectrom. Ion Processes* **1989**, *87*, 187−207.
(8) Fehsenfeld, F. C. *J. Chem. Phys.* **1971**, *54*, 438−439.
(9) Hunton, D. E.; Viggiano, A. A.; Swider, W.; Paulson, J. F.; Sherman, C. *J. Geophys. Res.* **1987**, *92*, 8827.
(10) Grabowski, J. J.; Van Doren, J. M.; DePuy, C. H.; Bierbaum, V. M. *J. Chem. Phys.* **1984**, *80*, 575−577.
(11) Viggiano, A. A.; Henchman, M. J.; Dale, F.; Deakyne, C. A.; Paulson, J. F. *J. Am. Chem. Soc.* **1992**, *114*, 4299.
(12) Le Page, V.; Keheyan, Y.; Snow, T. P.; Bierbaum, V. M. *J. Am. Chem. Soc.* **1999**, *121*, 9435−9446.
(13) Fehsenfeld, F. C.; Howard, C. J.; Ferguson, E. E. *J. Chem. Phys.* **1973**, *58*, 5841−5842.
(14) Arnold, S. T.; Miller, T. M.; Viggiano, A. A. *J. Phys. Chem. A* **2002**, *106*, 9900−9909.
(15) Viggiano, A. A.; Arnold, S. T.; Williams, S.; Miller, T. M. *Plasma Chem. Plasma Processes* **2002**, *22*, 285−295.
(16) Miller, T. M.; Arnold, S. T.; Viggiano, A. A. *Int. J. Mass Spectrom.* **2003**, *227*, 413−420.
(17) Arnold, S. T.; Miller, T. M.; Viggiano, A. A. *Int J. Mass Spectrom.* **2002**, *218*, 207−215.
(18) Irikura, K. K. *J. Chem. Phys.* **1995**, *102*, 5357.
(19) King, R. A.; Galbraith, J. M.; Schaefer, H. F. *J. Phys. Chem.* **1996**, *100*, 6061.
(20) Cheung, Y.-S.; Chen, Y.-J.; Ng, C. Y.; Chiu, S.-W.; Li, W.-K. *J. Am. Chem. Soc.* **1995**, *117*, 9725.
(21) Bauschlicher, C. W., Jr.; Ricca, A. *J. Phys. Chem. A* **1998**, *102*, 4722.
(22) McEwan, M. J.; Scott, G. B. I.; Adams, N. G.; Babcock, L. M.; Terzieva, R.; Herbst, E. *Astrophys. J.* **1999**, *513*, 287−293.
(23) Scott, G. B. I.; Fairley, D. A.; Freeman, C. G.; McEwan, M. J.; Spanel, P.; Smith, D. *J. Chem. Phys.* **1997**, *106*, 3982−3987.
(24) Scott, G. B. I.; Fairley, D. A.; Freeman, C. G.; McEwan, M. J.; Adams, N. G.; Babcock, L. M. *J. Phys. Chem. A* **1997**, *101*, 4973−4978.
(25) Barckholtz, C.; Snow, T. P.; Bierbaum, V. M. *Astrophys. J.* **2001**, *547*, L171−L174.
(26) Le Page, V.; Keheyan, Y.; Snow, T. P.; Bierbaum, V. M. *J. Am. Chem. Soc.* **1999**, *121*, 9435−9446.
(27) Le Page, V.; Keheyan, Y.; Snow, T. P.; Bierbaum, V. M. *Int J. Mass Spectrom.* **1999**, *185/186/187*, 949−959.
(28) Midey, A. J.; Miller, T. M.; Morris, R. A.; Viggiano, A. A. *J. Phys. Chem. A* **2005**, *109*, 2559−2563.
(29) Scott, G. B. I.; Milligan, D. B.; Fairley, D. A.; Freeman, C. G.; McEwan, M. J. *J. Chem. Phys.* **2000**, *112*, 4959−4965.
(30) Scott, G. B. I.; Fairley, D. A.; Milligan, D. B.; Freeman, C. G.; McEwan, M. J. *J. Phys. Chem. A* **1999**, *103*, 7470−7473.
(31) Scott, G. B. I.; Fairley, D. A.; Freeman, C. G.; McEwan, M. J.; Anicich, V. G. *J. Chem. Phys.* **1998**, *109*, 9010−9014.
(32) Scott, G. B. I.; Fairley, D. A.; Freeman, C. G.; McEwan, M. J. *Chem. Phys. Lett.* **1997**, *269*, 88−92.
(33) Scott, G. B. I.; Fairley, D. A.; Freeman, C. G.; McEwan, M. J. *J. Phys. Chem. A* **1999**, *103*, 1073−1077.
(34) Milligan, D. B.; McEwan, M. J. *Chem. Phys. Lett.* **2000**, *319*, 482−485.
(35) Milligan, D. B.; Fairley, D. A.; Freeman, C. G.; McEwan, M. J. *Int. J. Mass Spectrom.* **2000**, *202*, 351−361.
(36) Viggiano, A. A.; Howorka, F.; Albritton, D. L.; Fehsenfeld, F. C.; Adams, N. G.; Smith, D. *Astrophys. J.* **1980**, *236*, 492.
(37) Isoniemi, E.; Khriachtchev, L.; Lundell, J.; Rasanen, M. *J. Mol. Struct.* **2001**, *563−564*, 261−265.
(38) Isoniemi, E.; Khriachtchev, L.; Lundell, J.; Rasanen, M. *Phys. Chem. Chem. Phys.* **2002**, *4*, 1549−1554.
(39) Frank, A. J.; Sadilek, M.; Ferrier, J. G.; Turecek, F. *J. Am. Chem. Soc.* **1996**, *118*, 11321−11322.
(40) Frank, A. J.; Sadilek, M.; Ferrier, J. G.; Turecek, F. *J. Am. Chem. Soc.* **1997**, *119*, 12343−12353.
(41) Blitz, M. A.; Hughes, K. J.; Pilling, M. J.; Robertson, S. H. *J. Phys. Chem. A* **2006**, *110*, 2996−3009.
(42) Laakso, D.; Smith, C. E.; Goumri, A.; Rocha, J. D. R.; Marshall, P. *Chem. Phys. Lett.* **1994**, *227*, 377−383.
(43) Goumri, A.; Rocha, J. D. R.; Laakso, D.; Smith, C. E.; Marshall, P. *J. Phys. Chem. A* **1999**, *103*, 11328−11335.
(44) Qi, J. X.; Deng, W. Q.; Han, K. L.; He, G. Z. *J. Chem. Soc., Faraday Trans.* **1997**, *93*, 25−28.
(45) Ballester, M. Y.; Varandas, A. J. C. *Phys. Chem. Chem. Phys.* **2005**, *7*, 2305−2317.
(46) Binns, D.; Marshall, P. *J. Chem. Phys.* **1991**, *95*, 4940−4947.
(47) Morris, V. R.; Jackson, W. M. *Chem. Phys. Lett.* **1994**, *223*, 445−451.
(48) Denis, P. A.; Ventura, O. N. *Chem. Phys. Lett.* **2001**, *344*, 221−228.
(49) Napolion, B.; Watts, J. D. *Chem. Phys. Lett.* **2006**, *421*, 562−565.
(50) Viggiano, A. A.; Morris, R. A.; Dale, F.; Paulson, J. F.; Giles, K.; Smith, D.; Su, T. *J. Chem. Phys.* **1990**, *93*, 1149−1157.
(51) Fehsenfeld, F. C. Associative Detachment. In *Interactions Between Ions and Molecules*; Ausloos, P., Ed.; Plenum: New York, 1975; pp 387−412.
(52) Poutsma, J. C.; Midey, A. J.; Thompson, T. H.; Viggiano, A. A. *J. Phys. Chem. A* **2006**, *110*, 11315−11319.
(53) Poutsma, J. C.; Midey, A. J.; Viggiano, A. A. *J. Chem. Phys.* **2006**, *124*, 074301.
(54) Arnold, S. T.; Williams, S.; Dotan, I.; Midey, A. J.; Morris, R. A.; Viggiano, A. A. *J. Phys. Chem. A* **1999**, *103*, 8421−8432.
(55) *NIST Chemistry WebBook, NIST Standard Reference Database No. 69*; Linstrom, P. J., Mallard, W. G., Eds.; National Institutes of Standards and Technology: Gaithersburg, MD, June 2005; available online at http://webbook.nist.gov.
(56) Lobring, K. C.; Check, C. E.; Gilbert, T. M.; Sunderlin, L. S. *Int. J. Mass Spectrom.* **2003**, *227*, 361−372.
(57) Nimlos, M. R.; Ellision, G. B. *J. Phys. Chem.* **1986**, *90*, 2574−2580.
(58) Brinkmann, N. R.; Tschumper, G. S.; Schaefer, H. F., III. *J. Chem. Phys.* **1999**, *110*, 6240−6245.
(59) Forney, D.; Kellogg, C. B.; Thompson, W. E.; Jacox, M. E. *J. Chem. Phys.* **2000**, *113*, 86−97.

(60) Ferguson, E. E. *Chem. Phys. Lett.* **1983**, *99*, 89.

(61) Frisch, M. J.; Trucks, G. W.; Schlegel, H. B.; Scuseria, G. E.; Robb, M. A.; Cheeseman, J. R.; Montgomery, J. A., Jr.; Vreven, T.; Kudin, K. N.; Burant, J. C.; Millam, J. M.; Iyengar, S. S.; Tomasi, J.; Barone, V.; Mennucci, B.; Cossi, M.; Scalmani, G.; Rega, N.; Petersson, G. A.; Nakatsuji, H.; Hada, M.; Ehara, M.; Toyota, K.; Fukuda, R.; Hasegawa, J.; Ishida, M.; Nakajima, T.; Honda, Y.; Kitao, O.; Nakai, H.; Klene, M.; Li, X.; Knox, J. E.; Hratchian, H. P.; Cross, J. B.; Adamo, C.; Jaramillo, J.; Gomperts, R.; Stratmann, R. E.; Yazyev, O.; Austin, A. J.; Cammi, R.; Pomelli, C.; Ochterski, J. W.; Ayala, P. Y.; Morokuma, K.; Voth, G. A.; Salvador, P.; Dannenberg, J. J.; Zakrzewski, V. G.; Dapprich, S.; Daniels, A. D.; Strain, M. C.; Farkas, O.; Malick, D. K.; Rabuck, A. D.; Raghavachari, K.; Foresman, J. B.; Ortiz, J. V.; Cui, Q.; Baboul, A. G.; Clifford, S.; Cioslowski, J.; Stefanov, B. B.; Liu, G.; Liashenko, A.; Piskorz, P.; Komaromi, I.; Martin, R. L.; Fox, D. J.; Keith, T.; Al-Laham, M. A.; Peng, C. Y.; Nanayakkara, A.; Challacombe, M.; Gill, P. M. W.; Johnson, B.; Chen, W.; Wong, M. W.; Gonzalez, C.; Pople, J. A., *Gaussian 03W*, revision C.02; Gaussian, Inc.: Pittsburgh PA, 2003.

(62) Halstead, C. J.; Jenkins, D. R. *Trans. Faraday Soc.* **1969**, *65*, 3013.

(63) Durie, R. A.; Johnson, G. M.; Smith, M. Y. *Combust. Flame* **1971**, *17*, 197.

(64) Kallend, A. S. *Trans. Faraday Soc.* **1967**, *63*, 2442.

(65) Van Doren, J. M.; Friedman, J. F.; Miller, T. M.; Viggiano, A. A.; Denifl, S.; Scheier, P.; Mark, T. D.; Troe, J. *J. Chem. Phys.* **2006**, *124*, 124322.

(66) Fehsenfeld, F. C.; Schmeltekopf, A. L.; Schiff, H. I.; Ferguson, E. E. *Planet. Space Sci.* **1967**, *15*, 373.

(67) Fahey, D. W.; Bohringer, H.; Fehsenfeld, F. C.; Ferguson, E. E. *J. Chem. Phys.* **1982**, *76*, 1799.

(68) Williams, S.; Campos, M. F.; Midey, A. J.; Arnold, S. T.; Morris, R. A.; Viggiano, A. A. *J. Phys. Chem. A* **2002**, *106*, 997−1003.